Systemic, postsymptomatic antisense oligonucleotide rescues motor unit maturation delay in a new mouse model for type II/III spinal muscular atrophy

Laurent P. Bogdanik[a], Melissa A. Osborne[a], Crystal Davis[a], Whitney P. Martin[a], Andrew Austin[a], Frank Rigo[b], C. Frank Bennett[b], and Cathleen M. Lutz[a,1]

[a]Genetic Resource Science, The Jackson Laboratory, Bar Harbor, ME 04609; and [b]Isis Pharmaceuticals, Carlsbad, CA 92010

Edited by Thomas C. Südhof, Stanford University School of Medicine, Stanford, CA, and approved September 10, 2015 (received for review May 18, 2015)

Clinical presentation of spinal muscular atrophy (SMA) ranges from a neonatal-onset, very severe disease to an adult-onset, milder form. SMA is caused by the mutation of the *Survival Motor Neuron 1* (*SMN1*) gene, and prognosis inversely correlates with the number of copies of the *SMN2* gene, a human-specific homolog of *SMN1*. Despite progress in identifying potential therapies for the treatment of SMA, many questions remain including how late after onset treatments can still be effective and what the target tissues should be. These questions can be addressed in part with preclinical animal models; however, modeling the array of SMA severities in the mouse, which lacks *SMN2*, has proven challenging. We created a new mouse model for the intermediate forms of SMA presenting with a delay in neuromuscular junction maturation and a decrease in the number of functional motor units, all relevant to the clinical presentation of the disease. Using this new model, in combination with clinical electrophysiology methods, we found that administering systemically SMN-restoring antisense oligonucleotides (ASOs) at the age of onset can extend survival and rescue the neurological phenotypes. Furthermore, these effects were also achieved by administration of the ASOs late after onset, independent of the restoration of SMN in the spinal cord. Thus, by adding to the limited repertoire of existing mouse models for type II/III SMA, we demonstrate that ASO therapy can be effective even when administered after onset of the neurological symptoms, in young adult mice, and without being delivered into the central nervous system.

SMA | antisense oligonucleotide | neuromuscular junction | motor unit number estimation

Spinal muscular atrophy (SMA) is one of the leading causes of childhood mortality and the second most common autosomal recessive disorder, affecting between 1:6,000 and 1:10,000 live births (1). SMA is caused by loss-of-function mutations in the *SURVIVAL OF MOTOR NEURON 1* (*SMN1*) gene. In humans, an intrachromosomal duplication gives rise to an additional copy of the gene, called *SURVIVAL OF MOTOR NEURON 2* (*SMN2*), containing a single C-to-T transition in exon 7, which distinguishes it from *SMN1*. This transition results in the aberrant splicing of 80–90% of *SMN2* transcripts, causing them to skip exon 7 (2). Because a small fraction of the full-length, functional SMN protein is generated from *SMN2*, the range in disease severity correlates with the number of copies of the *SMN2* gene that a patient carries: One or two copies of *SMN2* are associated with the most severe (or type I) form of SMA, whereas three or four copies are associated with the mildest (or type III) form (3, 4). Although SMN is a ubiquitously expressed protein that plays a role in RNA processing, metabolism, and transport, deficiencies in SMN affect primarily the motor system. Because SMA is a disease of low levels of SMN (as opposed to complete lack of SMN) (5), it becomes a unique challenge to model the spectrum of disease severity in preclinical models.

Efficacy testing of SMA therapies has been primarily restricted to mouse models with very low levels of SMN, such as the Δ7 mouse, and is referred to as one of the "severe models," with a median survival of 12–14 d after birth (6–12). Attempts to generate a robust intermediate model have resulted in mice with near-normal life spans and little to no neuromuscular phenotype (13, 14). Although the severe models have been valuable research tools, their rapid phenotype progression presents several obstacles to preclinical testing of therapeutics. Among these is the narrow window for testing therapeutic interventions, as the short overall survival time of these mice limits the study of postonset interventions (11, 15–17). In these severe SMA mice, several studies have demonstrated that successful intervention in the disease course is limited to the early postnatal days (PNDs) (10, 17, 18). Whether this observation holds true in milder models of SMA remains to be answered but is a critical question, as type II/III patients represent the majority currently awaiting treatment. The severe models also do not represent the spectrum of disease severities observed in the patient population; the lack of efficacy of a potential therapy in the severe mouse model of SMA may not necessarily preclude its benefit in type II/III SMA patients. To further our understanding of therapeutic efficacy in the milder mouse models, longer lived mouse models are needed and must recapitulate hallmark features of the disease that can be used as outcome measures of potential therapies. These hallmark features include measurable SMN deficiency, the presence of human *SMN2* transgenes, and motor neuron defects that translate into functional deficits. Indeed, many SMA mouse models succumb to cardiac or circulatory phenotypes, which are not relevant

Significance

Spinal muscular atrophy (SMA) is one of the most frequent infantile genetic diseases and impairs breathing and locomotion. Promoting RNA splicing of one of the genes involved in SMA leads to spectacular improvements in laboratory models. Splicing modulators such as antisense oligonucleotides (ASOs) therefore come to the forefront of therapeutic candidates. However, timing of delivery and route of administration still need to be optimized. Do ASOs have to be delivered into the central nervous system, and are ASOs still efficient if administered late after disease onset? In a new mouse model for SMA, we show that ASOs were efficacious when delivered outside of the spinal cord and late after the onset of the symptoms of the animals.

Author contributions: L.P.B. and C.M.L. designed research; L.P.B., M.A.O., C.D., W.P.M., and A.A. performed research; F.R. and C.F.B. contributed new reagents/analytic tools; L.P.B. analyzed data; and L.P.B. and M.A.O. wrote the paper.

Conflict of interest statement: C.F.B. and F.R. are employees of Isis Pharmaceuticals. ISIS Pharmaceuticals is developing a SMN-targeting drug as a treatment for SMA.

This article is a PNAS Direct Submission.

Freely available online through the PNAS open access option.

[1]To whom correspondence should be addressed. Email: cat.lutz@jax.org.

This article contains supporting information online at www.pnas.org/lookup/suppl/doi:10.1073/pnas.1509758112/-/DCSupplemental.

to the clinical presentation (19). Although test compounds can extend the survival of these models, determining whether they reach and rescue neurological defects—the only ones with face validity—requires investigation beyond the most overt phenotypes such as shortened life span.

Several mouse models of SMA with life spans longer than that of the Δ7 mouse have been generated using various approaches. The *Smn2B*/– mouse model (20) and the SMN–read-through model (21) have a mean survival of 28–34 d. Milder SMA phenotypes have also been modeled by using selective ablation of SMN expression in critical tissues such as the skeletal muscle or the nervous system (22–24). These mouse mutants, with a median survival of 25 d, proved unequivocally that SMN is required in both the skeletal muscle and the motor neuron for the development of functional motor units. However, reduced SMN, as in SMA, and no SMN may have different physiological consequences as we have noted previously (5), and tissue-specific deletions of SMN might not present the optimal mechanistic validity required for preclinical models. Moreover, many of these mutants present an intrinsic limitation for preclinical studies: Because they do not carry the *SMN2* gene, they cannot be used to test potential therapies developed to increase the production of functional SMN protein by the *SMN2* copies carried by patients.

We recently characterized an allelic series of mouse models of SMA each with increasing copy numbers of human *SMN2* genetically engineered into the murine *Smn1* locus. In this set, the spectrum of phenotypes is very limited: Severe models are embryonic lethal, whereas very mild ones such as the $Smn1^{C/C}$ mouse (JAX stock no. 008604) have a near-normal life span with very mild neuromuscular deficits but a cardiac phenotype and necrosis (14). Therefore, we sought to generate an animal model for SMA that would have a lower expression of SMN than the very mild $Smn1^{C/C}$ model but survive beyond 1 mo of age, while focusing on preclinical endpoints more relevant to SMA than the sole survival or necrosis—namely, the maturation and function of the motor units. This new model allowed us to test the efficacy of antisense oligonucleotide (ASO) therapy administered at various time points after the onset of the phenotype and address the question of whether the efficacy of the rescue by these ASOs would correlate with a restoration of SMN levels in the spinal cord or in peripheral tissues. This question is important, as most therapies recently tested for SMA, a neurological disease, are painstakingly delivered into the central nervous system. We also tested whether surface electromyography, similar to the method used on patients, can serve the study of preclinical endpoints in this model.

Results

The Burgheron Mouse Model of SMA Type II/III.

Allelic composition and SMN protein levels. To generate a mouse model with a more severe reduction of SMN levels than the mild $Smn1^{C/C}$ model (14) but still reaching adulthood (about three months of age), we combined the following SMN alleles: the *SMN1* knockout created by M. Sendter, the SMN "C allele" created by Regeneron at the SMN locus, and the full-length human *SMN2* transgene created by A. Burghes (Fig. 1*A* and *Methods*). The C allele consists of the replacement of exons 7 and 8 from the mouse SMN locus by exons 7 and 8 of the human *SMN2* gene, in tandem with the insertion in the same locus but after the STOP codon of the murine SMN, of a full-length *SMN2* genomic fragment. As a tribute to the investigators who made these alleles available to the research community, we named our new

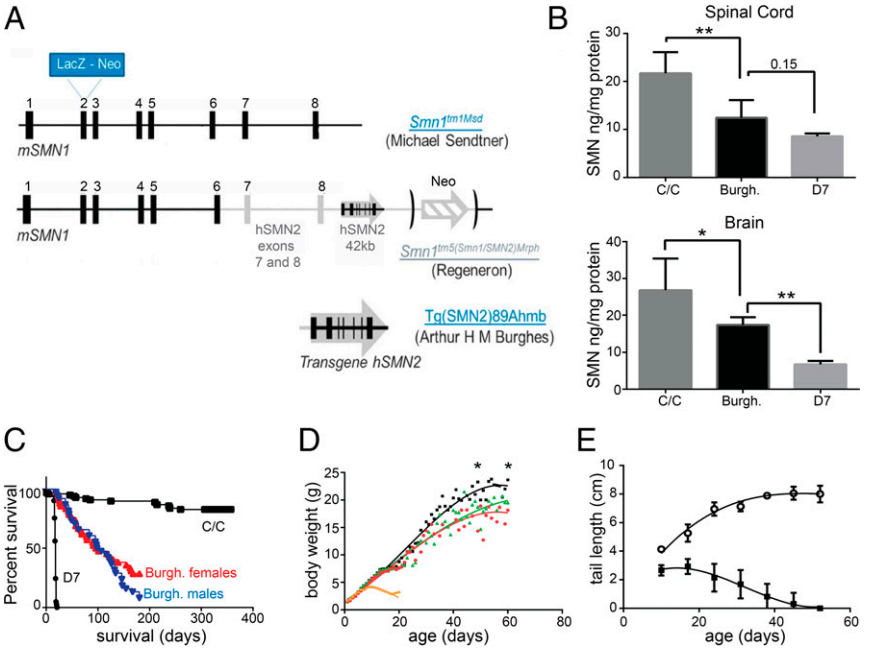

Fig. 1. Titration of the SMN protein and overt phenotypes of the Burgheron mutants. (*A*) The genetic make-up of the Burgheron mouse was as follows: The mutants are compound heterozygotes for the $Smn1^{tm1Msd}$ knockout of SMN1 from the Sendtner laboratory and the $Smn1^{tm5}$ (aka "C") allele from Regeneron; they also carry a single copy of the human $SMN2^{89Ahmb}$ transgene. (*B*) SMN protein expression in the Burgheron mutants, measured by ELISA, is lower than in SMN^{C} mutants but higher than in Δ7 mutants, in both the spinal cord and brain tissue, making the Burgheron mouse an intermediate SMA model. There was a very significant effect of the genotype on SMN levels; Burgheron mice were significantly different and displayed SMN levels intermediary between C/C and Δ7 mutants (Dunnett's multiple comparison tests, 0.15: $P = 0.15$). (*C*) Survival of Burgheron mice is longer than for Δ7 mice (median survival, 18 d) but shorter than for C/C mutants (median survival, >400 d; Mantel–Cox log-rank test, $P < 0.001$); there is no difference between the survival of male and female Burgheron mice ($P = 0.14$; median survival, 102 and 98.5 d, respectively). (*D*) Growth curves of control (WT, $n = 77$, black), C/C ($n = 100$, green), Bugheron ($n = 33$, red), and Δ7 ($n = 41$, orange) mice. Body weight (BW) at given ages were compared by Student *t* test, and major significance differences are indicated in the text. (*E*) Necrosis affects the tail of the Burgheron mutants as early as PND 10 (mutants, $n = 20$, black squares; littermate controls, $n = 38$, open circles).

model "Burgheron" [Jax Stock 14561 FVB.Cg-Tg(SMN2)89Ahmb *Smn1*^{tm1Msd} *Smn1*$^{tm5(Smn1/SMN2)Mrph}$/J].

We noted early on that a proportion of Burgheron mutants lived significantly longer than others despite being of identical genotype and gender. "Long-lived" mutants were born from matings where the Tg(SMN2)89Ahmb transgene and the *Smn1*^{tm1Msd} targeted mutation were paternally inherited and the *Smn1*^{C} allele was maternally inherited, a mating scheme that results in higher levels of SMN protein in the mutants than the reverse scheme (Fig. S1). Because of this observation, in subsequent analyses we used mutants only derived from matings yielding progeny with the lowest amount of SMN (*Methods*).

SMN proteins in the brain were quantified by ELISA (Fig. 1*B*). At 10 d of age, Burgheron mice expressed lower levels of SMN protein in the brain and spinal cord than the mild *Smn1*$^{C/C}$ mutant but higher levels than Δ7 mutants.

Survival. Relative to the severe Δ7 model for SMA (mean survival, 18 d) and to the mild *Smn1*$^{C/C}$ model (mean survival, >180 d), the Burgheron mutants, which are born at normal Mendelian ratios, demonstrated an intermediate life span with a mean survival time of 98.5 d for the females and 102 d for the males, with no significant gender difference (Mantel–Cox log-rank test, $P = 0.136$) (Fig. 1*C*). The growth curve of the Burgheron mice was slightly delayed compared with that of the *Smn1*$^{c/c}$ mice and wild-type mice during the first 2 wk of age, with the first significant difference observed at P6 (Burgheron, 3.43 g, $n = 24$; C/C, 3.92 g, $n = 80$; WT, 3.91 g, $n = 69$). From P9 on, however, Burgheron mice grew significantly bigger than Δ7 mice (Δ7, 4.19 g, $n = 36$; Burgheron, 5.02 g, $n = 27$). Growth curves of Burgheron and C/C mice became similar after P20, the first age where both mutants exhibited a slightly lower body weight (BW) than wild-type mice (Burgheron, 7.59 g, $n = 15$; C/C, 7.66 g, $n = 22$; WT, 8.75 g, $n = 20$) (Fig. 1*D*). By 2 mo of age, Burgheron and *Smn1*$^{c/c}$ mice displayed a similar BW, ∼20% lower than the control mice (Burgheron, 18.16 ± 1.53 g, $n = 9$; C/C, 19.5 ± 4.26 g, $n = 10$; WT, 23.65 ± 2.62 g, $n = 11$; $P < 0.05$).

Necrosis. Similar to other milder models of SMA (13, 25) and to severe models of SMA that have been therapeutically "rescued" (6, 11, 26), Burgheron mice develop necrosis in their tail, leading to complete tail loss by PND 45 (Fig. 1*E*). Necrosis progresses in a caudal-to-rostral fashion and progressively involves the hind feet as well as the ears. As with many models of SMA, limb necrosis is a confounding phenotype that prevented us from using standard neuromuscular assays such as rotarod, grip test, or gait analyses.

Cardiac abnormalities. Burgheron mutants succumbing in the survival study died abruptly and not of progressive neuromuscular decline. Multiple groups have reported some degree of cardiac dysfunction encompassing bradycardia, dilated cardiomyopathy with decreased contractility, and sympathetic innervation deficiency across multiple SMA mouse models (27–30). To assess cardiac function in Burgheron mice, we studied mutant and control mice by echocardiography and electrocardiography at PND 25, 35, 60, 90, and 120. We analyzed in two separate groups the mice that died "early" (before PND 89) or "late" (after PND 89). At each time point, the short-lived mutants displayed significantly lower heart rates ($P < 0.05$; *t* test) than the controls, whereas longer lived mutants only displayed a reduced heart beat after PND 35 (Fig. 2*A*). Short-lived Burgheron mutants also exhibited a significantly greater ratio of left ventricular mass normalized to BW (LVM:BW) than both the long-lived mutants and control mice from PND 25 on, whereas this defect only appeared after PND 60 in the long-lived mutants (Fig. 2*B*). Consistent with left ventricular hypertrophy (31) (Fig. 2*D*), systolic function was altered in the short-lived mutants, where ejection fraction (EF) was significantly lower (Fig. 2*C*). Upon necropsy, the heart of the Burgheron mutants was often found smaller in size, with a dilation of both ventricles and atria (Fig. 2*E*). Together, the observations of a severe cardiomyopathy in the mutants that die before the median survival age, but of a less severe cardiomyopathy in the mutants surviving past median survival age, suggest that these heart defects are causative of the death of the Burgheron mice.

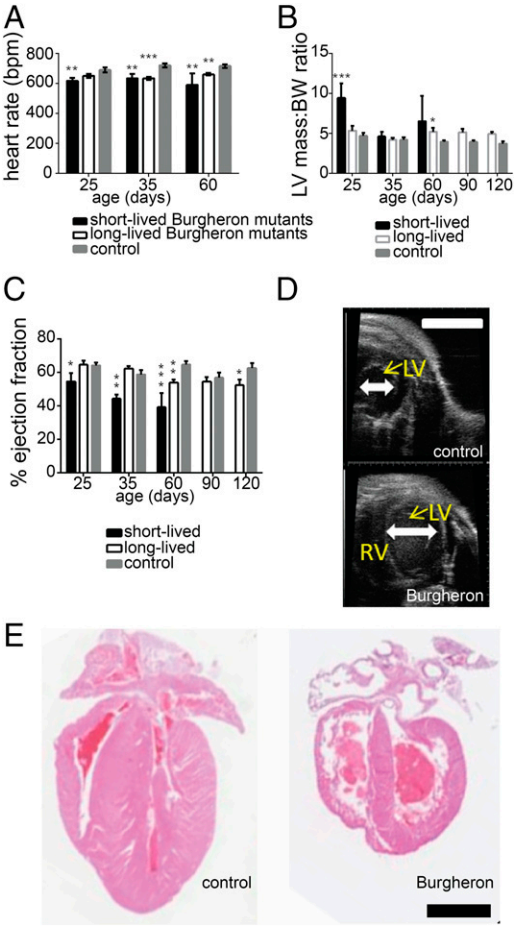

Fig. 2. Cardiac phenotype is likely the cause of the premature death of Burgheron mutants. Echocardiography was performed longitudinally from 25 to 120 d of age on mutants ($n = 17$) and wild-type ($n = 14$) mice. At the time of the analysis, mutants were separated into "short-lived" ($n = 7$) and long-lived ($n = 10$) cohorts depending on whether they had died before or after 89 d of age. (*A*) Heart rate. (*B*) Left ventricle mass normalized to BW. (*C*) EF (*A*–*C*, Dunnett's multiple comparison tests to the wild-type group). (*D*) Representative ultrasound images of the left ventricle of a mutant (*Bottom*) and control littermate (*Top*) at P35. (*E*) Representative hematoxylin/eosin staining of sagittal cross-sections of the heart of control (*Left*) and mutant (*Right*) mice at P35. The heart of the mutant mice was observed on animals euthanized for humane reasons, within less than a day before anticipated spontaneous death. [Scale bar, (*D* and *E*) 1 mm.]

Defective neuromuscular junction maturation. In the severe Δ7 mouse model of SMA, neuromuscular junction (NMJ) abnormalities are seen as early as PND 5 and consist in an accumulation of neurofilament proteins in the axon terminal, which fails to develop a complex terminal branching (32). "Vacant" endplates—that is, acetylcholine receptor (AChR) aggregates not connected by any terminal—were also observed (33). In models with a survival extended to 1 mo of age, such as the *Smn*$^{2B/-}$ mouse, another form of maturation delay was observed, with NMJ AChRs failing to develop a mature, perforated "pretzel" appearance and remaining in a disorganized plaque-like structure. Completely denervated NMJs were also observed (34). In both models, NMJs of postural, proximal muscles such as the transverse abdominis

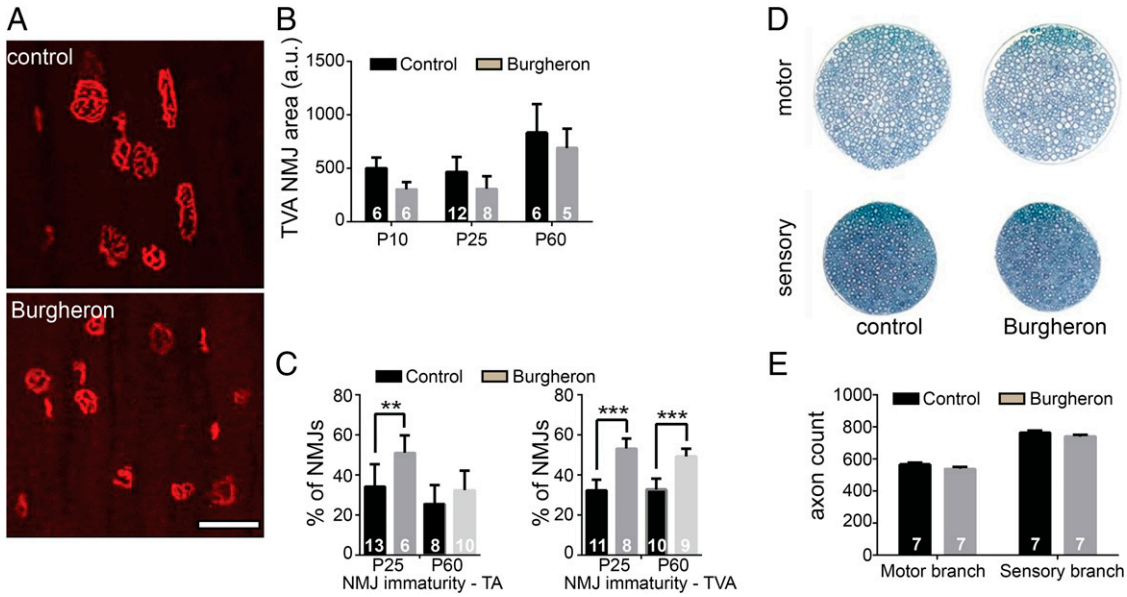

Fig. 3. NMJ maturation is delayed, but there is no axonal loss in the Burgheron mutants. (*A*) Representative NMJs stained with Alexa 594-conjugated alpha-bungarotoxin (BTX) on the TVA muscle of P35 mice. *Top*, control; *Bottom*, mutant. (Scale bar, 50 μm.) (*B*) Quantification of NMJ area in pixels from PND 10 to PND 60. There is a significant reduction in size of the NMJs in the mutants (two-way ANOVA for area, genotype, $P < 0.05$). (*C*) Percentage of immature NMJs in the TA and TVA muscles at PND 25 and PND 60 (Student *t* test between genotypes at different ages). (*D*) Femoral nerve representative pictures from PND 60 control (*Left*) and mutant (*Right*) mice. (*E*) Quantification of axon numbers in the motor and sensory branches of the femoral nerve at PND 60. (*B*, *C*, and *E*) Sample sizes indicated on graphs.

(TVA) were more affected than on other distal, leg muscles. Consistently, there is an NMJ phenotype in the Burgheron mutant that is more pronounced in the TVA than on leg muscles such as the tibialis anterior (TA) (Fig. 3*A*). At all ages observed, from PND 20 on, NMJs appeared smaller and less perforated, being closer in structure to the "plaque" form than to the pretzel shape (Fig. 3*A*). Burgheron mutants also had significantly smaller AChR clusters than control mice, at least from PND 10 to PND 60 (Fig. 3*B*). We used a "maturation index" to study the NMJ phenotype, whereby postsynaptic aggregates with less than two perforations (plaques) were counted as "immature," whereas endplates with three or more aggregates (pretzels) were counted as "mature." In the TVA, about 60% of the NMJ appeared immature at PND 25 in the mutants, and this delay in maturation persisted until at least PND 60 (Fig. 3*C*). In contrast, although about 50% of NMJs in the TA were immature at PND 25, the maturation was complete by PND 60, with a percentage of plaques identical in the mutant and control mice (Fig. 3*C*). Although the maturation of the NMJs was affected, we found no sign of denervation, such as retraction of the nerve terminal from the synaptic endplate, terminal sprouts, or disaggregation of the postsynaptic receptor aggregates. Moreover, the abnormal accumulation of neurofilament proteins in the nerve terminal, a hallmark of severe SMA mouse models (23), was absent in the Burgheron mutants (Fig. S2 *A–F*). Consistent with the absence of denervation, no atrophy of the skeletal muscle was observed; on average, muscle fibers were slightly smaller in the mutants than in control mice, as expected from their smaller size (Fig. S2 *G–J*).

In the most severe SMA models, as well as in type I and II SMA patients, peripheral axon loss has been observed. We found that axon numbers were identical in the motor and sensory branches of the femoral nerve of mutant and control mice at PND 60 (Fig. 3 *D* and *E*). Together, these observations indicate that, in the Burgheron mice, the maturation of the NMJs is impaired in the most affected muscles and that immature NMJs remain in a poorly differentiated state until late in life. However, there is no axonopathy detectable at the microscopic level.

Phenotype Rescue.

ASO-mediated restoration of SMN levels, both in adolescent and adult Burgheron mutants, corrects SMA-like and non–SMA-like phenotypes. The loss-of-function of SMN1 is embryonic lethal in mice, where, as in most mammals except humans, no *SMN2* gene exists to compensate for the loss of *SMN1*. When introduced by transgenesis, *SMN2* in mice functions as the endogenous *SMN2* gene in humans and is transcribed in majority into mRNAs lacking the seventh exon of the gene; they encode an unstable and nonfunctional protein. ASOs can modify the splicing of genes, and convergent studies have identified a short sequence in *SMN2* intron 7 acting as an intronic splicing silencer (named ISS-N1); the mutation of this sequence, as well as its masking by ASOs, increases the inclusion of exon 7 in *SMN2* mature mRNA and thereby the production of functional SMN protein (35, 36). By design, the Burgheron mice carry three copies of the human intron 7 (Fig. 1*A*). Therefore, they are well suited to pursue the in vivo characterization of ASOs targeting ISS-N1, initiated in severe models (16, 37).

Here, we tested the efficacy of ASO therapy after onset of the symptoms, with ASO or saline i.p. injections at either PND 10–12 or PND 25–28. The ASO used is uniformly modified with 2'-O-methoxyethyl nucleotides and a phosphorothioate backbone (*Methods*).

ASO therapy at PND 10 dramatically rescued the survival (Fig. 4*A*) and weight gain (Fig. 4*B*) of the Burgheron mutants until at least 180 d and 125 d of age, respectively. The necrosis of the tail was arrested by the treatment at PND 10 (Fig. 4*C*). Neuromuscular maturation was also rescued by PND 10 ASO therapy. Although the ratio of immature NMJs was identical in ASO-treated and vehicle-treated mutants at PND 25, by PND 60 the treated mutants displayed a ratio of mature NMJs identical to control mice (Fig. 4*D*).

ASO injection at PND 25 also significantly extended the survival and arrested the necrosis of the mutants (Fig. 4 *A* and *C*). However, PND 25 injection did not correct the lower BW gain observed in vehicle-treated mutants, and ASO-treated mice followed

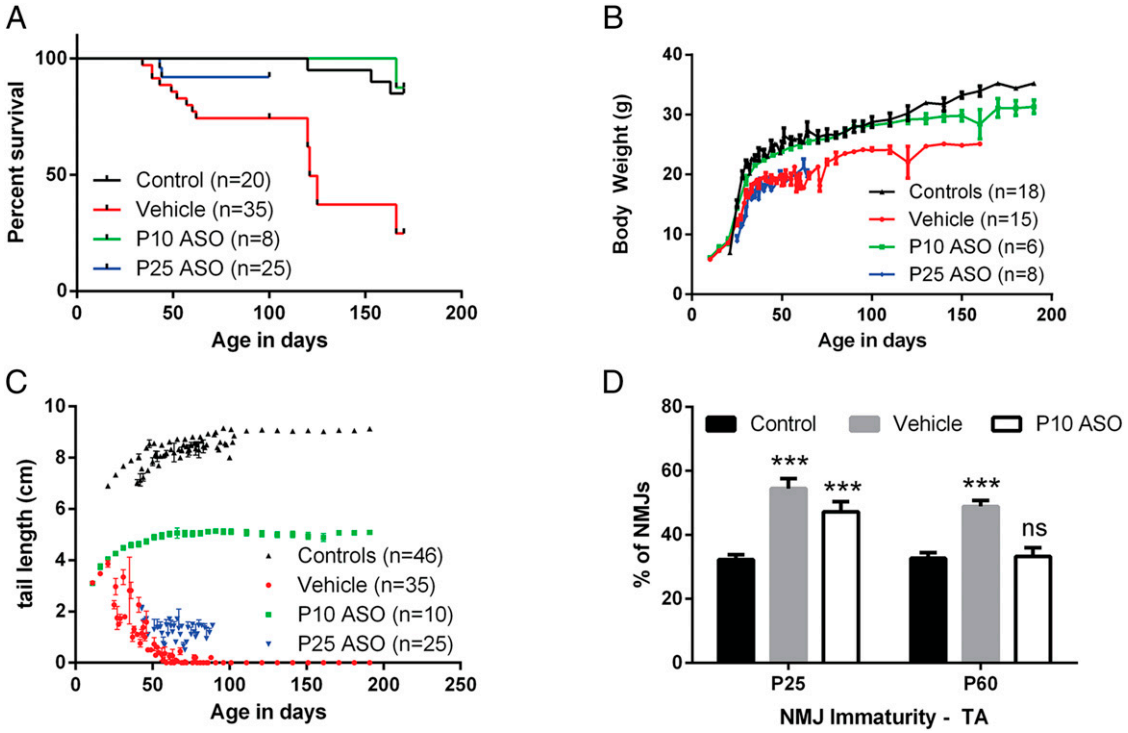

Fig. 4. ASO administration at PND 10 and PND 25 rescues lethality, necrosis, and NMJ maturation. (*A*) Survival curves of mutants injected with vehicle, ASO at PND 10, or ASO at PND 25 [log-rank (Mantel–Cox) test comparing to WT: vehicle, $P < 0.001$; ASO PND 10, $P = 0.82$; ASO PND 25, $P = 0.20$]. (*B* and *C*) Growth curve and tail length of mutants injected with vehicle, ASO at PND 10, or ASO at PND 25. (*D*) Percentage of NMJs on the TVA muscle presenting an immature profile after PND 10 ASO injection. NMJs were quantified at PND 25 and PND 60 in nonmutant control and vehicle- or ASO-treated mutant males. Sample size is indicated on the graph. Age ($P < 0.05$), experimental group ($P < 0.001$), and the interaction between both ($P < 0.05$) were significant (two-way ANOVA). There was a very significant increase in the percentage of immature NMJs in vehicle-treated mutants compared with controls at both PND 25 and PND 60 (Sidak's multiple comparison tests to control, $P < 0.001$). In ASO-treated mutants, the maturation was restored to wild-type levels at PND 60 (Sidak's multiple comparison tests to controls, n.s.) but not at PND 25 ($P < 0.001$).

the same growth as vehicle-treated mice from PND 25 to at least PND 80 (Fig. 4*B*).

The electrophysiology phenotype of the Burgheron mutants is rescued by peripheral ASO injection. Because lethality is likely caused by non-neuronal deficits such as the cardiac pathology in both the severe Δ7 model and the milder Burgheron model, the effect of ASOs on survival is not informative of their action on the nervous system. The rescue of the NMJ phenotype by treatment at PND 10, described above, is the first indication that systemic ASOs can restore the structure of at least the peripheral elements of the motor units. To address whether ASOs also have functional benefits, we turned to techniques increasingly used in the clinic for patient histories and clinical trials. Surface electromyography and motor unit number estimation (MUNE) (38–42) were used here to document the motor unit function in vivo.

Compound muscle action potential (CMAP) was reduced as early as PND 10 in the mutants to less than one-third of the wild-type amplitude (Fig. 5*A*). Incremental MUNE revealed that single motor unit potentials (SMUPs) were reduced to the same extent (Fig. 5*B*), and consequently, the average estimation of motor units was unchanged in the mutants. Over time, CMAP reduction persisted at PND 25, PND 35, and PND 60 in untreated Burgheron mice, being one-third lower than in controls by PND 60 (Fig. 5 *D* and *E*). Interestingly, ASO treatment at PND 10 caused a noticeable although not statistically significant recovery of the CMAP amplitude at both PND 25 and PND 60. PND 25 ASO administration had a more spectacular effect and significantly increased the CMAP recorded 10 d postinjection, at PND 35. The effect of the ASO was long lasting and still noted at PND 60. MUNE revealed fewer motor units in the mutants at PND 35 and PND 60. At both PND 35 and PND 60, the effects of an ASO administration at PND 25 rescued the motor unit supply to almost wild-type levels in treated mutants (Fig. 5*F*).

To document further the functioning of the NMJs, we used Repetitive Nerve Stimulation (RNS) at 3, 10, and 30 Hz. The phenotypes of the mutants consisted of decrements of the CMAP in response to the RNS. Notably, these abnormal decrements were observed at different frequencies at different ages. In PND 10 mutants, the 10-Hz stimulation caused a highly significant decrement in the mutants but not the control littermates (Fig. 5*G*). At PND 60, the 3-Hz and 30-Hz stimulations also unmasked decrements in the mutants that were absent (at 3 Hz) or less pronounced (at 30 Hz) in the wild-type littermates. In mutants that were administered the ASOs at PND 25—that is, 2 wk after the onset of the RNS phenotype onset observed at PND 10—RNS responses were rescued to wild-type levels (Fig. 5 *H* and *I*) by PND 60.

Rescue of the neurological phenotypes by ASOs does not correlate with an increase of SMN in the nervous system. Initial delivery of ASOs in the severe Δ7 model was performed by intracerebral ventricle injection with the goal to target motoneuron somas, from which the SMN-dependent neuropathy is believed to originate (37). However, later studies found that systemic (intraperitoneal) injections also rescue survival of severe SMA mouse models (16). These observations add to the long-lasting question of where SMN levels have to be critically restored to lead to phenotypic improvement and patient treatment. We found that systemic injection in the Burgheron mutants rescues the electrophysiology phenotype (Fig. 5). To test whether this treatment correlates with an increase of SMN in the central nervous system and the periphery, we measured full-length and Δ7 *SMN2* mRNAs in the

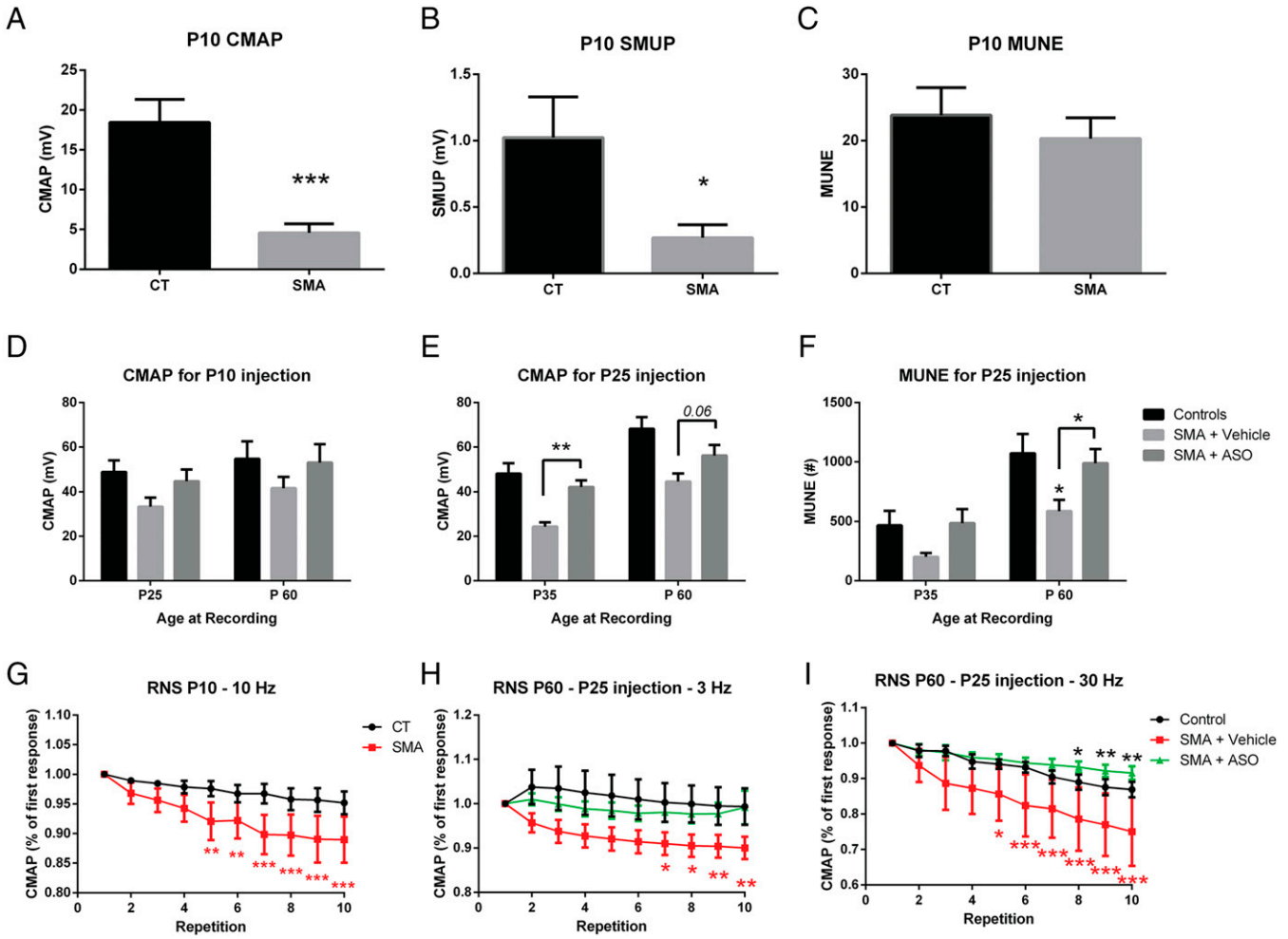

Fig. 5. Electrophysiology phenotype of the Burgheron mutants and rescue by ASO therapy. (*A–C*) Surface electromyography on PND 10 mutants ($n = 6$) and controls ($n = 6$) revealed a strongly reduced CMAP (*A*) and average SMUP (*B*) in the mutants. MUNE (*C*) was unchanged (Student *t* test). (*D* and *E*) CMAP was measured in control, vehicle-treated, and ASO-treated mutants ($n = 6$ per group) after ASO treatment at PND 10 (*D*) or PND 25 (*E*). Age at recording is indicated below the graphs. Effect of the treatment on mutants was almost significant after the PND 10 administration (two-way ANOVA, age, $P = 0.14$; treatment, $P = 0.054$) and highly significant after the PND 25 administration (two-way ANOVA, age, $P < 0.001$; treatment, $P < 0.001$). Significant differences between vehicle- and ASO-treated groups at a given age are indicated with brackets (Sidak's multiple comparison test). (*F*) On mice treated at PND 25, MUNE was highly affected by both the age ($P < 0.01$) and the treatment ($P < 0.001$, two-way ANOVA). At PND 60, MUNE was significantly lower in vehicle-treated mutants than in control mice ($*P < 0.05$) and restored in mutants treated at PND 25 (Sidak's multiple comparison test, bracket, $*P < 0.05$). (*G–I*) RNS at different frequencies revealed a strong decrement in the response (represented as a percentage of the first response) in the mutants (repeated-measure ANOVA, $P < 0.05$). ASO treatment at PND 25 prevented this decrement. Significant differences between the response to a given repetition and the initial response are indicated on the graph (two-way repeated-measure ANOVA, Dunnett's multiple comparison tests).

spinal cord and skeletal muscles of PND 60 mutants that had been injected with ASOs at either PND 10 or PND 25. ASO therapy at PND 10 resulted in a significant increase in the full-length/Δ7 mRNA ratio, with a more pronounced increase in the skeletal muscle (e.g., in the diaphragm; Fig. 6*A*) than in the spinal cord (Fig. 6*B*). SMN protein quantification by ELISA confirmed that injection of the ASOs at PND 10 resulted in a pronounced increase of SMN in the heart but little change in the brain, the spinal cord, and peripheral blood mononuclear cells (Fig. 6 *E–H*). PND 25 ASO therapy also resulted in a pronounced increase of the full-length/Δ7 mRNA ratio in muscles (Fig. 6*C*); this late injection had a very specific effect on muscles only, as no increase in the spinal cord was detected in PND 60-treated mutants (Fig. 6*D*).

Discussion

We present here an intermediate mouse model for SMA made by genetic titration of SMN levels. Overt features of this model include tail necrosis and cardiac abnormalities, however SMA-like defects were also found in the neuromuscular system. ASO therapy did improve the cardiac phenotype and, most likely as a consequence, extend survival. Because the cardiac defect has little relevance to the clinical presentation, we also focused our analyses on the rescue of the neurological phenotypes that we had identified.

The Burgheron mouse presents with a congestive heart failure phenotype, and we have provided several lines of evidence that indicate that this is the likely cause of premature death in the mutants: (*i*) Animals die abruptly, rather than with a progressive neurological decline, and (*ii*) significant changes in heart rate, LVM:BW ratio, and EF occur immediately before death. Instances of congenital heart defects have been reported in SMA patients, including heart malformation features (43–45). There have also been reports of patients exhibiting bradycardia (45) and a single case of necrosis of the digits and vascular thrombosis (46). Although involvement of the autonomic nervous system

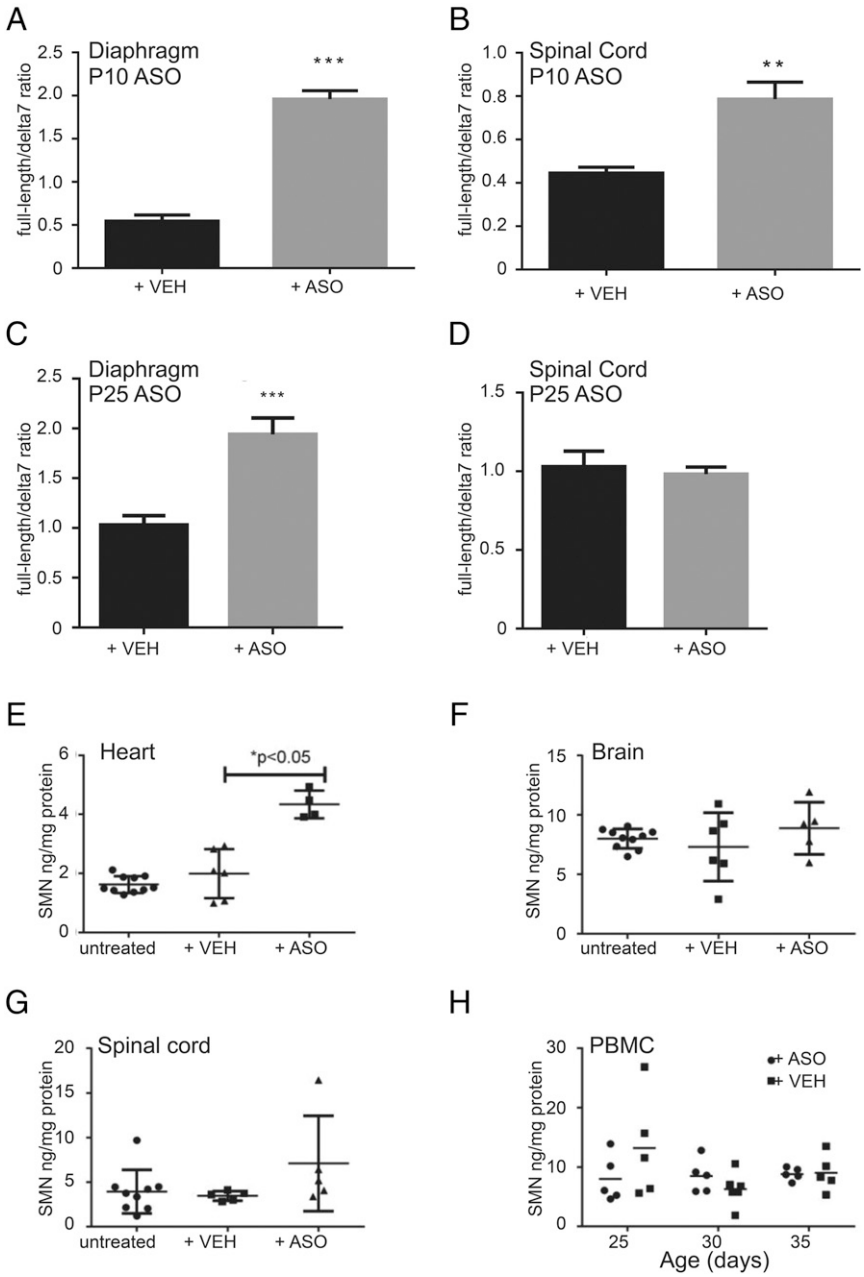

Fig. 6. Systemic ASO restores SMN RNA (*A–D*) and protein (*E–H*) levels in tissues including the spinal cord. Late administration increases SMN in muscles but not spinal cord. (*A* and *B*) *SMN2* mRNA quantification in the diaphragm (*A*) and spinal cord (*B*) of PND 60 mutants treated with vehicle or ASO at PND 10. The ratio of full-length (including exon 7) *SMN2* transcripts to *SMN2* transcripts lacking exon 7 (δ7) is shown. ASO-treated mutants had higher full-length *SMN2* expression in both tissues (Student *t* test, $n = 6$ per treatment group). (*C* and *D*) *SMN2* mRNA quantification in the diaphragm (*C*) and spinal cord (*D*) of PND 60 mutants. ASO treatment specifically increased full-length SMN mRNA levels in the diaphragm but not in the spinal cord (Student *t* test, $n = 6$ per treatment group). (*E–H*) SMN protein quantification by ELISA at PND 25 in untreated mutants ($n = 10$) or mutants treated at PND 10 with vehicle ($n = 6$) or ASO ($n = 5$). ASO treatment increased SMN protein in the heart only (Student *t* test between vehicle- and ASO-treated mutants). (*H*) SMN protein quantification in peripheral blood mononuclear cells (PBMCs) did not detect any increase following PND 10 administration of vehicle ($n = 5$) or ASO ($n = 5$). Measurements were performed at PND 25, 30, and 35.

and other organ systems in the pathogenesis of SMA have been called into question (30), cardiac defects are seldom part of the clinical presentation of SMA types I, II, and III (47). Cardiac defects are, however, the cause of death in both the severe SMA mouse models (29, 48) and milder models. This is a limitation of SMA mouse models that is well recognized (19), and caution should be used when circulatory phenotypes or survival in SMA mouse models are used as outcome measures of efficacy testing. Although they can be a readout for target engagement of SMN-restoring compounds, they are likely not informative of the window of opportunity and tissue requirement of SMN that are relevant to clinical testing. In our study, although we did not study the cardiac phenotype in ASO-treated mice, the extended survival and increased levels of SMN in the myocardium after treatment suggest that ASO therapy improves heart function in this mild SMA model. In more severe mouse models, systemic ASO delivery has also been shown to reverse the cardiac phenotype (16). The Burgheron mutants, therefore, like other long-lived SMA

models, could be used to further elucidate how low SMN levels affect either the sympathetic nervous system or the circulatory system, but relevant neurological phenotypes had to be identified and used as outcomes.

Burgheron mutants present a delay in the structural maturation of the NMJ endplates. This is reminiscent of the absence of perforation of the endplates in the 2B/– model (20). At the molecular level, postsynaptic maturation delay was also observed in more severe SMA models and consisted in the abnormal persistence after birth of embryonic (type gamma) AChR subunits at the NMJ (49). This delayed maturation calls for further investigation of the mechanisms driving the refinement of the endplates from the postnatal to the adult stages. Agrin, a major synaptic organizer, has been found to be less active in SMA models, and this partial loss of function could account for the maturation phenotype (50). However, synaptogenic agrin is transcribed in the motor neurons (51); we found that ASOs could restore the NMJ maturation independently of increasing SMN levels in the spinal cord. This raises the possibility that NMJ maturation in SMA relies in part on muscle- or Schwann cell-derived factors that remain to be identified.

In mice, surface electromyography, including MUNE, has been seldom used. Such tests were initially introduced to follow the progression of the denervation of leg muscles in amyotrophic lateral sclerosis (ALS) models (52–54), and only recently, MUNE was applied in the severe Δ7 SMA model (55) and the very mild C/C mouse (56). In both the ALS and Δ7 models, NMJ abnormalities have been observed, as well as a moderate (in Δ7 mice) to severe (in G93A mice) loss of peripheral axons. The electrophysiology phenotypes that were documented reflect the ability of this approach to detect major changes in the motor unit structural integrity. Whether CMAP measurement and MUNE are sensitive enough to detect milder motor unit defects in the mouse and whether mild SMA mouse models do display electrophysiological deficits have been little documented before. In the mild $Smn^{1C/C}$ mouse, CMAP, but not MUNE, was found to be reduced at 1 y of age (56). Our study provides the illustration of a MUNE deficit in a mild SMA model.

In type 2 and type 3 SMA, decreased MUNE is often found (41, 42) along with a decreased CMAP. Increased SMUP size has been reported in at least one study (41), suggesting that a compensatory reinnervation of denervated muscle fibers takes place in humans. Reductions of the CMAP and MUNE in the Burgheron mice are reminiscent of the human symptoms. SMUPs were not increased, which suggests that the compensatory motor unit enlargement observed in some patients does not occur in the Burgheron mice. This could be a consequence of the absence of frank denervation of the endplates. The absence of nerve pathology in the Burgheron mice, combined with their neurophysiology phenotype, points toward a pathology mechanism affecting either the NMJs, which could be silenced; the nerves, whose conduction could be blocked; or the postsynaptic muscle fibers, whose excitability could be reduced. Together, our findings suggest that anatomically normal motor units are silenced in the SMA mice. This is reminiscent of our previous finding that 8–15% of NMJs are structurally intact, yet silent, in the splenius capitis muscles of the $Smn1^{C/C}$ mouse at PND 90 and PND 350, respectively (14).

In this study, we explored the window of opportunity for therapeutic intervention in a mild SMA model. Systemic delivery at PND 0 and PND 3 of an ASO promoting the inclusion of *SMN2*'s exon 7 has proven spectacularly efficient in extending the median survival (from PND 10 to PND 108), as well as the NMJ maturation phenotype observed at PND 9, of a severe mouse model (16). Although mice that received only two injections at PND 1 and PND 3 developed necrosis, repeated s.c. injections also prevented this necrosis. We previously reported a postsymptomatic therapeutic window in the severe Δ7 mouse model, where restoration of SMN expression via a tamoxifen-inducible genetic rescue allele provided the greatest benefit with respect to survival if it was induced before PND 8 (17). Although the Δ7 mutants have a mean survival of 17 d, the Burgheron mutants, with a mean survival of 89 d, offered an unprecedented opportunity to test the efficacy of restoring SMN levels much later after the onset of the phenotype. In the present study, we found that late administration, in a milder model, also improves survival. Moreover, necrosis was stopped by only two successive administrations, either at PND 10 or PND 25.

In this study, we observed that ASO efficiency was age-dependent. When injected at PND 10, the ASO caused a noticeable, although not significant, recovery of the CMAP amplitude at both PND 25 and PND 60; but when injected at PND 25, the ASO had a more spectacular effect and significantly increased the CMAP recorded 10 d postinjection, at PND 35. Variation of the ASO biological effects with age could be related to changes in targeting efficiency or target abundance, as both the full-length and Δ7 mRNA expression change. Such an age dependency of ASO efficacy has been observed in another study with a different ASO. The increase in exon 7 inclusion in the liver, 2 d after injection, was found to be greater for injections performed at PND 8 or PND 13 than for injections performed at PND 2; later in age, the efficacy decreased for injections at PND 18 (57). For the ASOs used in our study, the age-dependent results seem to be shifted toward older ages, with efficacy being higher for injection in early adult (PND 25) than in younger mice (PND 10). This could be due to a critical treatment period (that remains to be defined) around PND 25, at a time when the PND 10 injection begins to wane, as ASO half-life in liver is ∼21 d (58).

To answer whether therapeutic ability is limited to presymptomatic stages or if it extends to a later time after the onset of the symptoms, the Burgheron model demonstrates here that treatment at the postsymptomatic age of PND 25, when NMJ maturation and electrophysiology of the motor unit are already affected, resulted in a robustly increased life span, arrested the necrotic phenotype, and restored a normal motor unit supply to the muscles.

Clinical trials for gene replacement and ASO therapies for SMA have begun, and drugs are being delivered systemically or in the central nervous system, respectively. Surprising evidence in mouse models, including this study, that peripheral ASOs can rescue the lethality and electrophysiology phenotypes raises the possibility that an alternative or additional delivery route could still be beneficial. They also question in which cell type SMN levels need to be restored in SMA. Although evident neuron loss is observed in type I SMA, supporting the role of SMN as a survival factor for motor neurons, it has been harder to identify in later-onset forms of the disease. In type II/III SMA, the role of glial cells and muscle cells in the maintenance and function of the motor unit remains to be explored. Few studies have focused on the role of the muscle, glial cells, and motoneurons themselves in the overall function of the motor units in SMA. Recently, the glial-specific restoration of SMN in mice with reduced SMN levels was found to be necessary to restore part of the motor unit function in a severe mouse model (59). In our study, peripheral administration of an ASO that rescues the SMA-like phenotypes of the NMJ and motor unit coincides with a better correction of *SMN2* splicing in the muscle than in the spinal cord and to a greater increase of SMN protein in the heart than in the brain or the spinal cord. This is consistent with the known inability of ASOs to cross the blood–brain barrier supports, which limits their effect, in our model, to the periphery of the nervous system. Previous studies and our present findings suggest at least two possible ways for peripheral ASOs to rescue SMN deficiency in the motor unit. On the one hand, SMN is known to regulate, in the liver, the secretion of Igf1, which does cross the blood–brain barrier and has a trophic function on spinal cord motoneurons (16).

In this scenario, peripheral ASOs would restore SMN in the liver and restore motoneuron function via the restoration of normal systemic growth factors. On the other hand, glial cells (and maybe muscle cells) are suspected to require a normal level of SMN to support the function of the motorunit (59); in this alternative but not exclusive scenario, peripheral ASOs would restore SMN in the Schwann cells of the peripheral nerves and restore the motor unit function. If this hypothesis is verified and translates to the human pathology, the skeletal muscle or the peripheral glia being involved in the disease would indicate that they may be target tissues for therapies. Additional studies are warranted to determine if these findings translate to SMA patients.

Methods

Generation of the Animal Model and Husbandry. SMA mutants (referred to here as Burgheron mutants) were created by crossing fully FVB/NJ congenic severe Burghes model female *SMN2*$^{+/+}$; *Smn1*$^{+/-}$ mice (JAX stock no. 007949) with fully FVB congenic males heterozygous for the previously described *Smn1*$^{C/-}$ allele (JAX stock no. 008604) (14) (*SI Methods*).

All experiments were conducted in accordance with the protocols described in the National Institutes of Health's *Guide for the Care and Use of Animals* (60) and were approved by The Jackson Laboratory Institutional Animal Care and Use Committee.

ASO Administration. Synthesis and purification of all chemically modified oligonucleotides were performed as previously described (58). ASO 10–29, 5′-ATTCACTTTCATAATGCTGG-3′, is uniformly modified with 2′-O-methoxyethyl nucleotides and a phosphorothioate backbone. It targets the ISS-N1 site (35). ASOs were dissolved in sterile PBS and injected i.p. at a dose of 80 μg/g BW twice, either at PND 10 and PND 12 or PND 25 and PND 27. For simplicity's sake, the experimental cohorts are referred to as injected at PND 10 or PND 25.

Survival and Phenotypic Assessment. Burgheron mutants were monitored for survival from birth through 6 mo of age. Mutants were weighed daily until weaning and once weekly thereafter.

Cardiac Assessment. Echocardiograms were recorded from anesthetized mice using a Vevo770 high-frequency ultrasound machine (VisualSonics). Mice were first anesthetized with 5% (vol/vol) isoflurane mixed with 100% oxygen at a flow of 1.0 L/min and were then maintained under anesthesia with a flow of 1.5% isoflurane/oxygen. Ophthalmic ointment was placed on the eyes to prevent drying of the cornea during anesthesia and ultrasound examination. Mouse heart rate and body temperature were monitored continuously during the procedure. After anesthetic induction, the animals were placed on a thermostatically controlled heated platform where isoflurane anesthesia was maintained by delivery through a close-fitting face mask. Heart rate was monitored through use of an electrocardiograph. Fur was removed from the ventral surface of the mouse torso with clippers and Nair (Church & Dwight). The 2D (B-mode), M-mode, and Doppler images were acquired from modified parasternal long-axis view, parasternal short-axis view, suprasternal notch view, and apical three-chamber view. The heart rate, fractional shortening, EF, stroke volume, and cardiac output were obtained for cardiac function assessment. Qualitative and quantitative measurements were made postimaging using VevoStrain analytic software.

NMJ Phenotyping. NMJ imaging was performed as described previously (61, 62) and as detailed in *SI Methods*.

NMJs were analyzed across three areas of the TVA or TA muscle endplate from three to six mutants and controls at PND 10, 25, and 60. Sections were analyzed at 20× magnification. NMJs within each section were defined as "on their side" (noninformative), plaque (<2 perforations), or pretzel (numerous perforations). The maturation index was calculated as the percentage of immature (plaque-like) NMJs over the total number of informative NMJs.

Peripheral Axon Counts. For peripheral axon counts, the sensory and motor branches of the femoral nerve were dissected above the medial quadriceps femoris and fixed in 2% (wt/vol) glutaraldehyde, 2% (wt/vol) paraformaldehyde, and 0.1 M cacodylate buffer overnight at 4°. Both nerve branches were embedded in plastic, and 0.5-μm sections were cut and stained with toluidine blue. Photomicrographs were analyzed semiautomatically as described previously (60) with the ImageJ software. Counts of myelinated axons in the motor and the sensory branches were reported.

Surface Electromyography. For surface electromyography, mice were anesthetized with isoflurane (5% induction, 2% maintenance), and internal body temperature was maintained at 37° with a homeothermic controller and plate (AD Instruments, cat. no. ML295/m) coupled to a rectal probe. The method previously described (53) was adapted as described in *SI Methods*.

SMN Alternative Splicing Quantitative Real-Time PCR. Total RNA was extracted from diaphragm and spinal cord tissue samples with the Zymo Research Direct-Zol RNA Miniprep Kit (cat. no. R2052), and 800 ng of diaphragm RNA or 400 ng of spinal cord RNA was reverse-transcribed to cDNA using random hexamers with the Life Technologies High Capacity cDNA Reverse Transcription Kit (cat. no. 4368813). RNA yields and quality were assessed with a NanoDrop ND-1000 spectrophotometer. Following standard protocols, quantitative real-time PCR was performed with custom-designed assays (*SI Methods*). Fold changes to control samples were calculated in the mutants using the ΔΔCt method for full-length and Δ7 mRNAs. GAPDH was used as the reference gene. Full-length Δ7 ratios were calculated with these fold changes.

SMN ELISAs. SMN levels were assessed in the indicated tissue homogenates using a commercially available SMN ELISA Kit (cat. no. ADI-900–209; Enzo Life Sciences) according to the manufacturer's protocol. This ELISA was developed by the SMA community as an improved alternative to Western blots (63). This kit detects both human and mouse SMN protein. Briefly, tissues were disrupted using a mechanical homogenizer, cellular debris was pelleted via centrifugation at 12,000 × *g* for 10 min, and the supernatant was transferred to a clean tube and assayed for protein concentration using Bio-Rad DC Protein Assay (cat. no. 500–011EDU). Protein lysates were prediluted before assaying according to the manufacturer's protocol.

Statistics. Statistical significance of Student *t* test, ANOVA, two-way ANOVA, and post hoc multicomparison Dunnett's and Sidak's tests is indicated on the graph as follows: $*P < 0.05$, $**P < 0.01$, $***P < 0.001$.

ACKNOWLEDGMENTS. We thank the highly trained animal care technicians and colony managers for their hard work and dedication with special thanks to Randy Walls, Amy Leighton, and Jonathan Newell. We would also like to thank the SMA mouse community for the generous sharing of resources and amazing collaborative spirit. Special thanks to Dione Kobayashi for her advice and strong support over the years. This work was funded by the SMA Foundation and National Institute of Neurological Disorders and Stroke Grant R21NS078251 (to C.M.L.).

1. Pearn J (1978) Incidence, prevalence, and gene frequency studies of chronic childhood spinal muscular atrophy. *J Med Genet* 15(6):409–413.
2. Lorson CL, Hahnen E, Androphy EJ, Wirth B (1999) A single nucleotide in the SMN gene regulates splicing and is responsible for spinal muscular atrophy. *Proc Natl Acad Sci USA* 96(11):6307–6311.
3. Feldkötter M, Schwarzer V, Wirth R, Wienker TF, Wirth B (2002) Quantitative analyses of SMN1 and SMN2 based on real-time lightCycler PCR: Fast and highly reliable carrier testing and prediction of severity of spinal muscular atrophy. *Am J Hum Genet* 70(2):358–368.
4. Lefebvre S, et al. (1997) Correlation between severity and SMN protein level in spinal muscular atrophy. *Nat Genet* 16(3):265–269.
5. Le TT, et al. (2005) SMNDelta7, the major product of the centromeric survival motor neuron (SMN2) gene, extends survival in mice with spinal muscular atrophy and associates with full-length SMN. *Hum Mol Genet* 14(6):845–857.
6. Avila AM, et al. (2007) Trichostatin A increases SMN expression and survival in a mouse model of spinal muscular atrophy. *J Clin Invest* 117(3):659–671.
7. Butchbach MER, et al. (2010) Effects of 2,4-diaminoquinazoline derivatives on SMN expression and phenotype in a mouse model for spinal muscular atrophy. *Hum Mol Genet* 19(3):454–467.
8. Chang J-G, et al. (2001) Treatment of spinal muscular atrophy by sodium butyrate. *Proc Natl Acad Sci USA* 98(17):9808–9813.
9. Narver HL, et al. (2008) Sustained improvement of spinal muscular atrophy mice treated with trichostatin A plus nutrition. *Ann Neurol* 64(4):465–470.
10. Naryshkin NA, et al. (2014) Motor neuron disease. SMN2 splicing modifiers improve motor function and longevity in mice with spinal muscular atrophy. *Science* 345(6197):688–693.
11. Passini MA, et al. (2010) CNS-targeted gene therapy improves survival and motor function in a mouse model of spinal muscular atrophy. *J Clin Invest* 120(4):1253–1264.
12. Riessland M, et al. (2010) SAHA ameliorates the SMA phenotype in two mouse models for spinal muscular atrophy. *Hum Mol Genet* 19(8):1492–1506.

13. Hsieh-Li HM, et al. (2000) A mouse model for spinal muscular atrophy. *Nat Genet* 24(1):66–70.
14. Osborne M, et al. (2012) Characterization of behavioral and neuromuscular junction phenotypes in a novel allelic series of SMA mouse models. *Hum Mol Genet* 21(20): 4431–4447.
15. Gogliotti RG, et al. (2013) The DcpS inhibitor RG3039 improves survival, function and motor unit pathologies in two SMA mouse models. *Hum Mol Genet* 22(20): 4084–4101.
16. Hua Y, et al. (2011) Peripheral SMN restoration is essential for long-term rescue of a severe spinal muscular atrophy mouse model. *Nature* 478(7367):123–126.
17. Lutz CM, et al. (2011) Postsymptomatic restoration of SMN rescues the disease phenotype in a mouse model of severe spinal muscular atrophy. *J Clin Invest* 121(8): 3029–3041.
18. Le TT, et al. (2011) Temporal requirement for high SMN expression in SMA mice. *Hum Mol Genet* 20(18):3578–3591.
19. Iascone DM, Henderson CE, Lee JC (2015) Spinal muscular atrophy: From tissue specificity to therapeutic strategies. *F1000Prime Rep* 7:04.
20. Bowerman M, Murray LM, Beauvais A, Pinheiro B, Kothary R (2012) A critical SMN threshold in mice dictates onset of an intermediate spinal muscular atrophy phenotype associated with a distinct neuromuscular junction pathology. *Neuromuscul Disord* 22(3):263–276.
21. Mattis VB, Bowerman M, Kothary R, Lorson CL (2008) A SMNDelta7 read-through product confers functionality to the SMNDelta7 protein. *Neurosci Lett* 442(1):54–58.
22. Cifuentes-Diaz C, et al. (2001) Deletion of murine SMN exon 7 directed to skeletal muscle leads to severe muscular dystrophy. *J Cell Biol* 152(5):1107–1114.
23. Cifuentes-Diaz C, et al. (2002) Neurofilament accumulation at the motor endplate and lack of axonal sprouting in a spinal muscular atrophy mouse model. *Hum Mol Genet* 11(12):1439–1447.
24. Frugier T, et al. (2000) Nuclear targeting defect of SMN lacking the C-terminus in a mouse model of spinal muscular atrophy. *Hum Mol Genet* 9(5):849–858.
25. Monani UR, et al. (2003) A transgene carrying an A2G missense mutation in the SMN gene modulates phenotypic severity in mice with severe (type I) spinal muscular atrophy. *J Cell Biol* 160(1):41–52.
26. Gavrilina TO, et al. (2008) Neuronal SMN expression corrects spinal muscular atrophy in severe SMA mice while muscle-specific SMN expression has no phenotypic effect. *Hum Mol Genet* 17(8):1063–1075.
27. Bevan AK, et al. (2010) Early heart failure in the SMNDelta7 model of spinal muscular atrophy and correction by postnatal scAAV9-SMN delivery. *Hum Mol Genet* 19(20): 3895–3905.
28. Cobb MS, et al. (2013) Development and characterization of an SMN2-based intermediate mouse model of Spinal Muscular Atrophy. *Hum Mol Genet* 22(9): 1843–1855.
29. Heier CR, Satta R, Lutz C, DiDonato CJ (2010) Arrhythmia and cardiac defects are a feature of spinal muscular atrophy model mice. *Hum Mol Genet* 19(20):3906–3918.
30. Shababi M, et al. (2012) Partial restoration of cardio-vascular defects in a rescued severe model of spinal muscular atrophy. *J Mol Cell Cardiol* 52(5):1074–1082.
31. Lorell BH, Carabello BA (2000) Left ventricular hypertrophy: Pathogenesis, detection, and prognosis. *Circulation* 102(4):470–479.
32. Kariya S, et al. (2008) Reduced SMN protein impairs maturation of the neuromuscular junctions in mouse models of spinal muscular atrophy. *Hum Mol Genet* 17(16): 2552–2569.
33. Murray LM, et al. (2008) Selective vulnerability of motor neurons and dissociation of pre- and post-synaptic pathology at the neuromuscular junction in mouse models of spinal muscular atrophy. *Hum Mol Genet* 17(7):949–962.
34. Murray LM, Beauvais A, Bhanot K, Kothary R (2013) Defects in neuromuscular junction remodelling in the Smn(2B/-) mouse model of spinal muscular atrophy. *Neurobiol Dis* 49:57–67.
35. Hua Y, Vickers TA, Okunola HL, Bennett CF, Krainer AR (2008) Antisense masking of an hnRNP A1/A2 intronic splicing silencer corrects SMN2 splicing in transgenic mice. *Am J Hum Genet* 82(4):834–848.
36. Singh NK, Singh NN, Androphy EJ, Singh RN (2006) Splicing of a critical exon of human Survival Motor Neuron is regulated by a unique silencer element located in the last intron. *Mol Cell Biol* 26(4):1333–1346.
37. Passini MA, et al. (2011) Antisense oligonucleotides delivered to the mouse CNS ameliorate symptoms of severe spinal muscular atrophy. *Sci Transl Med* 3(72):72ra18.
38. McComas AJ, Fawcett PR, Campbell MJ, Sica RE (1971) Electrophysiological estimation of the number of motor units within a human muscle. *J Neurol Neurosurg Psychiatry* 34(2):121–131.
39. Bromberg MB (2004) Motor unit number estimation: New techniques and new uses. *Suppl Clin Neurophysiol* 57:120–136.
40. Gooch CL, Shefner JM (2004) ALS surrogate markers. MUNE. *Amyotroph Lateral Scler Other Motor Neuron Disord* 5(Suppl 1):104–107.
41. Kang PB, et al.; Muscle Study Group and the Pediatric Neuromuscular Clinical Research Network for Spinal Muscular Atrophy (2014) The motor neuron response to SMN1 deficiency in spinal muscular atrophy. *Muscle Nerve* 49(5):636–644.
42. Swoboda KJ, et al. (2005) Natural history of denervation in SMA: Relation to age, SMN2 copy number, and function. *Ann Neurol* 57(5):704–712.
43. Møller P, et al. (1990) Spinal muscular atrophy type I combined with atrial septal defect in three sibs. *Clin Genet* 38(2):81–83.
44. Bürglen L, et al. (1995) SMN gene deletion in variant of infantile spinal muscular atrophy. *Lancet* 346(8970):316–317.
45. Bach JR (2007) Medical considerations of long-term survival of Werdnig-Hoffmann disease. *Am J Phys Med Rehabil* 86(5):349–355.
46. Rudnik-Schöneborn S, et al. (2010) Digital necroses and vascular thrombosis in severe spinal muscular atrophy. *Muscle Nerve* 42(1):144–147.
47. Palladino A, et al. (2011) Cardiac involvement in patients with spinal muscular atrophies. *Acta Myol* 30(3):175–178.
48. Shababi M, et al. (2010) Cardiac defects contribute to the pathology of spinal muscular atrophy models. *Hum Mol Genet* 19(20):4059–4071.
49. Kong L, et al. (2009) Impaired synaptic vesicle release and immaturity of neuromuscular junctions in spinal muscular atrophy mice. *J Neurosci* 29(3):842–851.
50. Zhang Z, et al. (2013) Dysregulation of synaptogenesis genes antecedes motor neuron pathology in spinal muscular atrophy. *Proc Natl Acad Sci USA* 110(48):19348–19353.
51. Burgess RW, Nguyen QT, Son YJ, Lichtman JW, Sanes JR (1999) Alternatively spliced isoforms of nerve- and muscle-derived agrin: Their roles at the neuromuscular junction. *Neuron* 23(1):33–44.
52. Shefner JM (2001) Motor unit number estimation in human neurological diseases and animal models. *Clin Neurophysiol* 112(6):955–964.
53. Shefner JM, Cudkowicz ME, Brown RH, Jr (2002) Comparison of incremental with multipoint MUNE methods in transgenic ALS mice. *Muscle Nerve* 25(1):39–42.
54. Shefner JM, Cudkowicz M, Brown RH, Jr (2006) Motor unit number estimation predicts disease onset and survival in a transgenic mouse model of amyotrophic lateral sclerosis. *Muscle Nerve* 34(5):603–607.
55. Arnold WD, et al. (2014) Electrophysiological biomarkers in spinal muscular atrophy: Preclinical proof of concept. *Ann Clin Transl Neurol* 1(1):34–44.
56. Li J, et al. (2014) A comparison of three electrophysiological methods for the assessment of disease status in a mild spinal muscular atrophy mouse model. *PLoS One* 9(10):e111428.
57. Keil JM, et al. (2014) A short antisense oligonucleotide ameliorates symptoms of severe mouse models of spinal muscular atrophy. *Mol Ther Nucleic Acids* 3(7):e174.
58. Rigo F, et al. (2014) Pharmacology of a central nervous system delivered 2′-O-methoxyethyl-modified survival of motor neuron splicing oligonucleotide in mice and nonhuman primates. *J Pharmacol Exp Ther* 350(1):46–55.
59. McGovern VL, et al. (2015) SMN expression is required in motor neurons to rescue electrophysiological deficits in the SMNΔ7 mouse model of SMA. *Hum Mol Genet* ddv283, 10.1093/hmg/ddv283.
60. National Research Council (1996) *Guide for the Care and Use of Laboratory Animals* (Public Health Service, Washington, DC), 7th Ed.
61. Bogdanik LP, et al. (2013) Loss of the E3 ubiquitin ligase LRSAM1 sensitizes peripheral axons to degeneration in a mouse model of Charcot-Marie-Tooth disease. *Dis Model Mech* 6(3):780–792.
62. Burgess RW, Cox GA, Seburn KL (2010) Neuromuscular disease models and analysis. *Methods Mol Biol* 602:347–393.
63. Kobayashi DT, et al. (2011) Utility of survival motor neuron ELISA for spinal muscular atrophy clinical and preclinical analyses. *PLoS One* 6(8):e24269.
64. Monani UR, et al. (2000) The human centromeric survival motor neuron gene (SMN2) rescues embryonic lethality in Smn(-/-) mice and results in a mouse with spinal muscular atrophy. *Hum Mol Genet* 9(3):333–339.
65. Schrank B, et al. (1997) Inactivation of the survival motor neuron gene, a candidate gene for human spinal muscular atrophy, leads to massive cell death in early mouse embryos. *Proc Natl Acad Sci USA* 94(18):9920–9925.
66. Lomen-Hoerth C, Olney RK (2000) Comparison of multiple point and statistical motor unit number estimation. *Muscle Nerve* 23(10):1525–1533.